Density induced phase transitions in QED_2 - A study with matrix product states

Mari Carmen Bañuls,[1] Krzysztof Cichy,[2,3] J. Ignacio Cirac,[1] Karl Jansen,[4] and Stefan Kühn[1]

[1] *Max-Planck-Institut für Quantenoptik, Hans-Kopfermann-Straße 1, 85748 Garching, Germany*
[2] *Goethe-Universität Frankfurt am Main, Institut für Theoretische Physik, Max-von-Laue-Straße 1, 60438 Frankfurt am Main, Germany*
[3] *Faculty of Physics, Adam Mickiewicz University, Umultowska 85, 61-614 Poznań, Poland*
[4] *NIC, DESY Zeuthen, Platanenallee 6, 15738 Zeuthen, Germany*

(Dated: November 3, 2016)

We numerically study the zero temperature phase structure of the multi-flavor Schwinger model at non-zero chemical potential. Using matrix product states, we reproduce analytical results for the phase structure for two flavors in the massless case and extend the computation to the massive case, where no analytical predictions are available. Our calculations allow us to locate phase transitions in the mass-chemical potential plane with great precision, and provide a concrete example of tensor networks overcoming the sign problem in a lattice gauge theory calculation.

Gauge theories are a fundamental concept in high energy physics. Nevertheless in many cases, such as quantum chromodynamics (QCD), they are notoriously hard and a full analytical solution seems to be impossible. Following the pioneering work by Wilson [1], lattice gauge theory (LGT) has become a standard tool for attacking gauge theories in the non-perturbative regime. This discretized formulation on a Euclidean space-time lattice enabled powerful Monte Carlo (MC) simulations that allowed the determination of phase diagrams, mass spectra and other properties. However, the sign problem [2] prevents accessing certain parameter regimes with this technique, as for example large parts of the phase diagram for QCD with chemical potential. Moreover, real-time dynamics are mostly inaccessible, despite some recent progress enabling the study of dynamics in particular regimes [3]. Consequently, there is an enduring search for alternative approaches overcoming these limitations [4–6], among them MC on Lefshetz thimbles, complex Langevin methods and density of states methods. A different line of research is quantum simulation of gauge theories. During recent years a number of works have analyzed this possibility [7–11] and even performed some experimental realization for small systems [12].

In the last decade, a new generation of methods based on tensor networks (TN) has revealed itself as a powerful approach for the non-perturbative study of quantum many body systems (see Ref. [13] for a review), both bosonic and fermionic, without suffering from a sign problem. In the context of LGT, they can be used to approximate the partition function in a Lagrangian formulation [14–16], but their main power can be exploited in the Hamiltonian formulation, thanks to their capability to efficiently describe the relevant states of the theory [17–24]. In recent years there has been significant theoretical progress with the development of gauge invariant TN formulations suitable for LGT [11, 25–29], as well as numerical simulations showing the power of the method for spectral calculations [17, 18, 30], thermal states [19–21], exploring phase diagrams [22, 31] and simulating real-time evolution for Abelian as well as non-Abelian theories [18, 23, 24].

Some of the works mentioned above achieved precisions beyond the reach of MC calculations for the considered models in one spatial dimension. Extending this success to higher spatial dimensions, although conceptually possible, is not an immediate task in the general case, but in regimes where MC simulations suffer from the sign problem, TN techniques should provide a very general solution. This major promise can already be demonstrated in the one-dimensional case, a task that we tackle in this letter. We study numerically the multi-flavor Schwinger model at non-zero chemical potential, and perform a full calculation in regimes where MC would suffer from a sign problem [32]. We go through the full extrapolation procedure to recover the continuum limit to explicitly show the power of TN approaches for overcoming the sign problem.

For the two-flavor case with equal masses for both flavors, on which we focus here, the model has an SU(2) isospin symmetry between the flavors and is in many aspects similar to QCD as it shows confinement, an anomalous U(1) current in the massless limit and a non-vanishing chiral condensate. The phase structure was determined analytically in Refs. [33, 34], where it was found that at zero temperature the model supports an infinite number of phases characterized by the isospin number and separated by first-order phase transitions.

Here, we numerically study the Hamiltonian lattice formulation of the model with MPS and carry out the extrapolation to the continuum limit. As a first necessary step, we reproduce the analytical prediction for massless fermions from Refs. [33, 34] with great precision. Furthermore, our calculation can be readily extended to the massive case, where no analytical computations are available. For the massive case we observe that the phase structure of the model changes significantly. Using the MPS approach, and considering the case of vanishing background field, we are able to map out accurately the phase diagram of the model in the mass - chemical potential plane for fixed volume. Our results thus constitute

an explicit demonstration that MPS allow reliable numerical simulations in a regime where the MC approach would suffer from the sign problem.

We adopt a lattice formulation with Kogut-Susskind staggered fermions [35]. In the temporal gauge, and in absence of a background field, the Hamiltonian for F flavors on a lattice with spacing a and N sites reads

$$\begin{aligned} H = &- \frac{i}{2a} \sum_{n=0}^{N-2} \sum_{f=0}^{F-1} \left(\phi_{n,f}^\dagger e^{i\theta_n} \phi_{n+1,f} - \text{h.c.} \right) \\ &+ \sum_{n=0}^{N-1} \sum_{f=0}^{F-1} \left(m_f (-1)^n + \kappa_f \right) \phi_{n,f}^\dagger \phi_{n,f} \\ &+ \frac{ag^2}{2} \sum_{n=0}^{N-2} L_n^2. \end{aligned} \tag{1}$$

In the expression above, $\phi_{n,f}$ is a single component fermionic field describing a fermion of flavor f on site n, and m_f/g and κ_f/g are the corresponding mass and the chemical potential in units of the coupling constant, g. The operators L_n and θ_n act on the gauge links in between the fermions and L_n gives the quantized electric flux on link n. They fulfill the commutation relation $[\theta_n, L_m] = i\delta_{n,m}$ and hence $e^{i\theta_n}$ acts as rising operator for the electric flux. We work with a compact formulation, where θ_n is restricted to $[0, 2\pi]$ [36].

Physical states, $|\psi\rangle$, have to satisfy the Gauss law, $G_n|\psi\rangle = 0 \ \forall n$, where G_n are the generators for gauge transformations, given by $G_n = L_n - L_{n-1} - \sum_{f=0}^{F-1} \left(\phi_{n,f}^\dagger \phi_{n,f} - \frac{1}{2}(1-(-1)^n) \right)$. For open boundary conditions (OBC), this allows us to integrate out the gauge fields. Assuming zero electric field on the left boundary, applying a residual gauge transformation and with a rescaling that makes it dimensionless [37], the Hamiltonian (1) can be finally written as

$$\begin{aligned} W = &- ix \sum_{n=0}^{N-2} \sum_{f=0}^{F-1} \left(\phi_{n,f}^\dagger \phi_{n+1,f} - \text{h.c.} \right) \\ &+ \sum_{n=0}^{N-1} \sum_{f=0}^{F-1} \left(\mu_f (-1)^n + \nu_f \right) \phi_{n,f}^\dagger \phi_{n,f} \\ &+ \sum_{n=0}^{N-2} \left(\sum_{k=0}^{n} \left(\sum_{f=0}^{F-1} \phi_{k,f}^\dagger \phi_{k,f} - \frac{F}{2}(1-(-1)^k) \right) \right)^2, \end{aligned} \tag{2}$$

where the adimensional parameters of the problem are $x = 1/(ag)^2$, $\mu_f = 2\sqrt{x} m_f/g$ and $\nu_f = 2\sqrt{x}\kappa_f/g$. In the following, we will focus on the case of two flavors in the sector of vanishing total charge, for which the conventional MC approach in general suffers from the sign problem [38].

Our variational ansatz is a MPS with OBC. For N sites this is a state of the form

$$|\psi\rangle = \sum_{i_0, i_1, \ldots i_{N-1}} A_0^{i_0} A_1^{i_1} \ldots A_{N-1}^{i_{N-1}} |i_0\rangle \otimes \cdots \otimes |i_{N-1}\rangle.$$

In the previous expression $|i_k\rangle_{i_k=1}^d$ is a basis for the Hilbert space on site k, $A_k^{i_k}$ are complex $D \times D$ matrices for $0 < k < N-1$ and $A_0^{i_0}$ ($A_{N-1}^{i_{N-1}}$) is a D-dimensional row (column) vector. The parameter D which determines the number of variational parameters and limits the maximum entanglement that can be present in the state, is called the bond dimension of the MPS (see e.g. Ref. [13]).

In order to show that MPS allow for reliable calculations with proper continuum limit in the regime of the sign problem, we first reproduce the analytical predictions for the massless case from Refs. [33, 34], which studied the continuum model in a fixed volume. To compare to these results, we consider lattices of constant volume, $Lg = N/\sqrt{x}$. The isospin number on the lattice is given by $\Delta N = N_0 - N_1$, with $N_i = \sum_{n=0}^{N-1} \phi_{n,i}^\dagger \phi_{n,i}$. It can be easily shown that the Hamiltonian (2) up to a constant only depends on the difference between the chemical potentials, $\nu_1 - \nu_0$, commonly called the isospin chemical potential in the literature (see Appendix). Thus we study ΔN in the ground state as a function of the difference between the chemical potentials. Following Refs. [33, 34], we define the rescaled isospin chemical potential $\mu_I/2\pi = N/4\pi x \cdot (\nu_1 - \nu_0)$, and hereafter we fix $\nu_0 = 0$ and only vary ν_1. We are thus studying the model in a situation where MC suffers from the sign problem. To probe for possible finite volume effects, we explore several volumes, $Lg = 2, 6, 8$.

In order to be able to extrapolate to the continuum limit, we study several lattice spacings corresponding to $x \in [9, 121]$. MPS calculations are subject to a truncation error due to the limited bond dimension reachable, bounded by the computational cost of treating too large matrices in the variational ansatz. To control this truncation error for each combination of $(Lg, x, \mu_I/2\pi)$, we repeat the computation for several bond dimensions, $D \in [40, 220]$, and extrapolate to $D \to \infty$ (see Appendix for details on the extrapolation procedure). Although MPS and TN in general can describe fermionic degrees of freedom, in the one-dimensional case it is convenient for the numerical simulations to map Eq. (2) to a spin chain by a Jordan-Wigner transformation (details about the spin formulation are given in the Appendix).

The results for the massless case are shown in Fig. 1. As $\mu_I/2\pi$ is increased, the value of ΔN exhibits discontinuous changes, by two units. For different isospin number the lowest energy levels are different, too. Hence, a crossing of these lowest energy levels corresponds to a change in isospin number. This leads to an abrupt change of the nature of the ground state, indicated by first-order (discontinuous) quantum phase transitions between phases characterized by their isospin number. The

location of the phase transition is determined by the position of the energy cusps on the $\mu_I/2\pi$ axis, as seen in the upper inset of Fig. 1. Repeating the calculations for several lattice spacings, we can estimate the continuum phase structure of the model (see Appendix for more details). For the first two transitions, our continuum estimates do not show any volume dependence, in agreement with Refs. [33, 34]. However, for transitions between phases with larger ΔN, we can see that for volume $Lg = 2$ there are deviations due to finite volume effects, which disappear for a larger volume, $Lg = 6$, for which we recover the analytical results in the entire parameter regime under study. We conclude that the transitions occur for $\mu_I/2\pi$ values which are odd multiples of $1/2$, in agreement with the analytical results. The finite volume effects found in our MPS calculation for small Lg can be explained because the total fermion number coincides with the number of sites, $N_0 + N_1 = N$. Hence, the system size ultimately upper bounds N_i and larger values for ΔN at fixed volume would require larger system sizes and correspondingly larger values of x to reach the correct continuum limit.

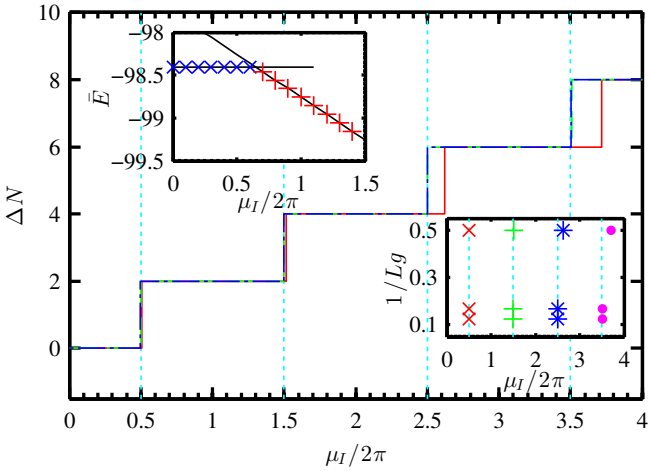

FIG. 1. (Color online) Upper inset: Close-up around the first transition for the ground state energy as a function of $\mu_I/2\pi$ for $Lg = 8$, $x = 16$, $m/g = 0$ and $D = 160$. The black lines show the predictions for $\Delta N = 0$ and $\Delta N = 2$, the markers the ground state energies obtained by our MPS calculation, where blue ✕'s indicate $\Delta N = 0$ and red crosses $\Delta N = 2$. Lower inset: Continuum estimate of the location of the phase transition versus inverse volume for the first (red ✕'s), second (green crosses), third (blue asterisks) and fourth (magenta dots) transition. Main plot: Continuum estimate for ΔN as a function of $\mu_I/2\pi$, for volumes 2 (red solid line), 6 (green dashed line) and 8 (blue dash-dotted line). The (dotted) vertical lines indicate the theoretical prediction for the phase transitions in the massless case.

While the analytical calculation in Refs. [33, 34] is limited to the massless case, the MPS formalism can deal with (arbitrary) mass values. Repeating the same calculations and extrapolation procedure for $m/g = 0.5$, we obtain the results shown in Fig. 2. Comparing Figs. 1 and 2, we observe that the new energy scale introduced by m/g leads to a change in the phase structure, as the locations of the first-order phase transitions are not equidistantly spaced anymore. The continuum estimates show a clear dependence on the volume, even for the first phase transition, and the size of the plateaus is no longer equal.

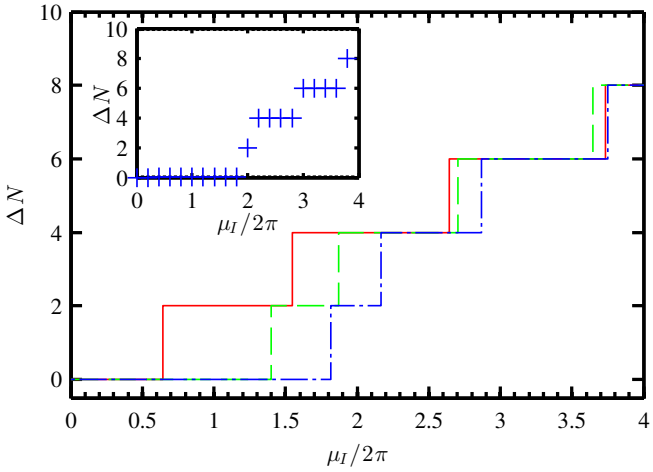

FIG. 2. (Color online) Inset: Isospin number as a function of $\mu_I/2\pi$ for $Lg = 8$, $x = 121$, $m/g = 0.5$ and $D = 220$. Main plot: Continuum estimate for ΔN as a function of $\mu_I/2\pi$, for volumes 2 (red solid line), 6 (green dashed line) and 8 (blue dash-dotted line).

Computing the phase structure for several masses, we can map out the phase diagram for the model in the m/g - $\mu_I/2\pi$ plane for a fixed volume. Fig. 3 shows the results for volume $Lg = 8$. One can see that for larger masses the phase characterized by $\Delta N = 0$ survives up to noticeably larger values of $\mu_I/2\pi$ and the size of the region for the $\Delta N = 2$ phase shrinks for larger masses. The regions describing phases with larger values for ΔN are less affected and only slightly bend towards higher values of the chemical potential difference. This behavior can be understood qualitatively as follows: The energy eigenvalues inside each phase only depend on the chemical potential difference, up to a constant (see inset of Fig. 1 and Appendix). This constant is mass dependent, and comparing its value at non-zero m/g to the massless case, we observe larger changes for phases characterized by a small isospin number. Consequently the locations of the level crossings, and hence the locations of the phase transitions, are shifted, especially for phases characterized by small ΔN (see Appendix for more details).

A further advantage of the MPS method is that not only it is free from the sign problem, but at the end of the computation it yields the ground state wave function, hence giving easy access to any observables that can be expressed as matrix product opera-

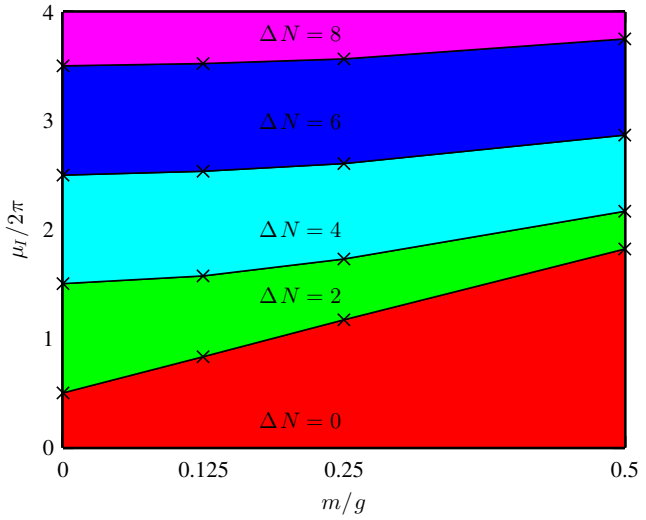

FIG. 3. (Color online) Phase diagram in the m/g - $\mu_I/2\pi$ plane for volume $Lg = 8$. The different colors indicate the regions for the different phases characterized by different values of ΔN. The black ✕'s mark the data points obtained after the extrapolation procedure.

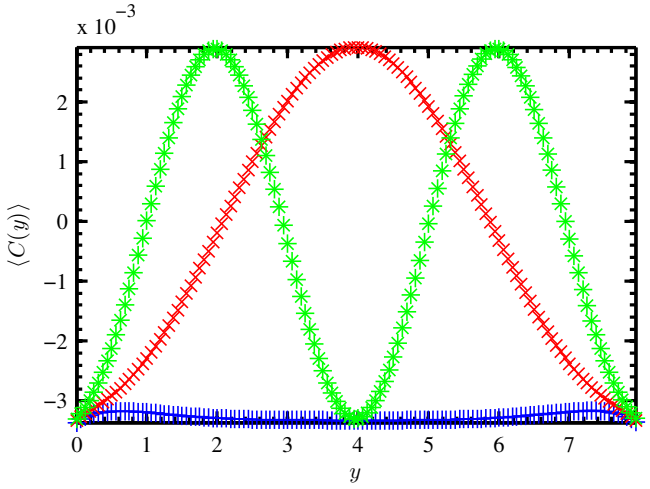

FIG. 4. (Color online) Expectation value of the chiral condensate as a function of position for $Lg = 8$, $x = 1024$, $m/g = 0$ and $D = 160$. The different curves correspond to different phases, where the blue crosses represent $\Delta N = 0$, the red ✕'s $\Delta N = 2$ and the green asterisks $\Delta N = 4$.

tors [39]. An interesting observable is the chiral condensate. Previous studies [40–42] for the (single-flavor) Schwinger model found that at finite density the chiral condensate shows spatial inhomogeneities of the form $\langle\bar{\psi}(y)\psi(y)\rangle = \langle\bar{\psi}\psi\rangle_0 \cos(2\kappa y)$, where ψ is a two component Dirac spinor, κ is the chemical potential, y the position and $\langle\bar{\psi}\psi\rangle_0$ the (spatially homogeneous) expectation value of the chiral condensate for vanishing chemical potential. Later work instead argued that these oscillations occur due to the breaking of translational invariance in finite systems [43]. With the MPS approach we can address this question, too. To be able to connect our staggered lattice calculation to the continuum, we sum the contribution of an even and its neighboring odd site to the chiral condensate and look at $C(y = 2n/\sqrt{x}) = \sum_{f=0}^{F-1}(C_{n,f} + C_{n+1,f})$, n even, where $C_{n,f} = \frac{\sqrt{x}}{N}(-1)^n \phi^\dagger_{n,f}\phi_{n,f}$ [44]. The result for $Lg = 8$ in the massless case is shown in Fig. 4. The value at zero density (corresponding to the $\Delta N = 0$ phase) is homogeneous up to small finite size effects at the boundaries, as expected from the theoretical result. For phases at non-zero density (given by $\Delta N \neq 0$) the condensate starts to oscillate sinusoidally, as expected for a finite system breaking translational invariance, and we observe an increase in the oscillation frequency with increasing density. The oscillation amplitudes are close to $\langle C(y)\rangle_0$, similar to the theoretical predictions from Refs. [40–43] for the single-flavor case. A more detailed study of the oscillations in the chiral condensate is beyond the scope of this paper and will be shown elsewhere [45].

In summary, we have shown a successful lattice calculation in the regime where the conventional MC approach suffers from the sign problem. Our results for the massless case in a sufficiently large volume agree with great precision with the analytical calculations from Refs. [33, 34], and we recover the predicted phase structure and locations of the phase transitions after extrapolating to the continuum limit. Furthermore, our calculations can be immediately extended to the massive case, where no analytical results are available. In this case, the observed phase structure is significantly different, and the locations of the phase transitions are no longer independent of Lg. We can map out the phase diagram of the model at a fixed volume in the m/g - $\mu_I/2\pi$ plane, and we see that the transition from $\Delta N = 0$ to $\Delta N = 2$ is significantly shifted towards higher values of the chemical potential at the expense of the phase characterized by $\Delta N = 2$. Phases with larger values of ΔN are apparently less affected and only slightly shifted towards higher values of $\mu_I/2\pi$ for increasing mass. Our results for the condensate are very similar to the theoretical predictions for the single-flavor case at non-zero density. We observe oscillations with a density dependent frequency around zero with an amplitude close to the zero density condensate value.

In our study, we focused on the phases at zero background field and temperature, with non-vanishing chemical potential, in order to explore a regime that suffers from the sign problem in conventional MC calculations. Notice, however, that the model also exhibits interesting features in other parameter regimes. In particular, in the absence of chemical potential and background field, it has been shown to have a second order phase transition for zero fermion mass at $T_c = 0$ [46, 47]. It might also show

a transition, similar to the single flavor case, at non vanishing background field, as has been argued in Ref. [48]. Adding a background field as well as a generalization to non-zero temperature [19–21] is straightforward, hence these regimes are also amenable to tensor network studies.

Although we have studied the two-flavor case, the MPS approach can be easily extended to an arbitrary number of flavors as shown in the Appendix. Furthermore, with the MPS approach it is to some extent possible to simulate real time evolution [18], thus making it possible to address also dynamical aspects of the model. Moreover, our results can serve as a test bench for other methods trying to overcome the sign problem.

Acknowledgments. K.C. was supported by the Deutsche Forschungsgemeinschaft (DFG), project nr. CI 236/1-1 (Sachbeihilfe).

[1] K. G. Wilson, Phys. Rev. D **10**, 2445 (1974).
[2] M. Troyer and U.-J. Wiese, Phys. Rev. Lett. **94**, 170201 (2005).
[3] F. Hebenstreit, J. Berges, and D. Gelfand, Phys. Rev. Lett. **111**, 201601 (2013).
[4] M. Cristoforetti, F. Di Renzo, A. Mukherjee, and L. Scorzato, Phys. Rev. D **88**, 051501 (2013).
[5] C. Gattringer and K. Langfeld, International Journal of Modern Physics A **31**, 1643007 (2016).
[6] A. Ammon, T. Hartung, K. Jansen, H. Leövey, and J. Volmer, arXiv:1607.05027 (2016).
[7] D. Banerjee *et al.*, Phys. Rev. Lett. **109**, 175302 (2012).
[8] U.-J. Wiese, Annalen der Physik **525**, 777 (2013).
[9] S. Kühn, J. I. Cirac, and M.-C. Bañuls, Phys. Rev. A **90**, 042305 (2014).
[10] E. Zohar, J. I. Cirac, and B. Reznik, Reports on Progress in Physics **79**, 014401 (2016).
[11] M. Dalmonte and S. Montangero, Contemporary Physics **57**, 388 (2016).
[12] E. A. Martinez *et al.*, Nature **534**, 516–519 (2016).
[13] F. Verstraete, V. Murg, and J. Cirac, Adv. Phys. **57**, 143 (2008).
[14] S. Takeda and Y. Yoshimura, Progress of Theoretical and Experimental Physics **2015** (2015).
[15] A. Denbleyker *et al.*, Phys. Rev. D **89**, 016008 (2014).
[16] Y. Shimizu and Y. Kuramashi, Phys. Rev. D **90**, 014508 (2014).
[17] M. C. Bañuls, K. Cichy, K. Jansen, and J. I. Cirac, JHEP (2013).
[18] B. Buyens, J. Haegeman, K. Van Acoleyen, H. Verschelde, and F. Verstraete, Phys. Rev. Lett. **113**, 091601 (2014).
[19] M. C. Bañuls, K. Cichy, J. I. Cirac, K. Jansen, and H. Saito, Phys. Rev. D **92**, 034519 (2015).
[20] M. C. Bañuls, K. Cichy, K. Jansen, and H. Saito, Phys. Rev. D **93**, 094512 (2016).
[21] B. Buyens, F. Verstraete, and K. Van Acoleyen, Phys. Rev. D **94**, 085018 (2016).
[22] P. Silvi, E. Rico, M. Dalmonte, F. Tschirsich, and S. Montangero, arXiv:1606.05510 (2016).
[23] S. Kühn, E. Zohar, J. Cirac, and M. C. Bañuls, Journal of High Energy Physics **2015**, 1 (2015).
[24] T. Pichler, M. Dalmonte, E. Rico, P. Zoller, and S. Montangero, Phys. Rev. X **6**, 011023 (2016).
[25] E. Rico, T. Pichler, M. Dalmonte, P. Zoller, and S. Montangero, Phys. Rev. Lett. **112**, 201601 (2014).
[26] P. Silvi, E. Rico, T. Calarco, and S. Montangero, New Journal of Physics **16**, 103015 (2014).
[27] E. Zohar and M. Burrello, New Journal of Physics **18**, 043008 (2016).
[28] L. Tagliacozzo, A. Celi, and M. Lewenstein, Phys. Rev. X **4**, 041024 (2014).
[29] J. Haegeman, K. Van Acoleyen, N. Schuch, J. I. Cirac, and F. Verstraete, Phys. Rev. X **5**, 011024 (2015).
[30] B. Buyens, J. Haegeman, K. Van Acoleyen, and F. Verstraete, PoS(LATTICE2014)308 (2014).
[31] E. Zohar, M. Burrello, T. B. Wahl, and J. I. Cirac, Annals of Physics **363**, 385 (2015).
[32] It has been noticed that in certain restricted parameter regimes the sign problem can be circumvented [49], but here we adopt a general prescription, common for massless and massive cases, where that is not the case.
[33] R. Narayanan, Phys. Rev. D **86**, 125008 (2012).
[34] R. Lohmayer and R. Narayanan, Phys. Rev. D **88**, 105030 (2013).
[35] J. Kogut and L. Susskind, Phys. Rev. D **11**, 395 (1975).
[36] C. J. Hamer, Z. Weihong, and J. Oitmaa, Phys. Rev. D **56**, 55 (1997).
[37] T. Banks, L. Susskind, and J. Kogut, Phys. Rev. D **13**, 1043 (1976).
[38] In the special case $\nu_0 + \nu_1 = 0$ the sign problem can be circumvented [33].
[39] I. P. McCulloch, Journal of Statistical Mechanics: Theory and Experiment **2007**, P10014 (2007).
[40] W. Fischler, J. Kogut, and L. Susskind, Phys. Rev. D **19**, 1188 (1979).
[41] Y.-C. Kao and Y.-W. Lee, Phys. Rev. D **50**, 1165 (1994).
[42] H. R. Christiansen and F. A. Schaposnik, Phys. Rev. D **53**, 3260 (1996).
[43] M. A. Metlitski, Phys. Rev. D **75**, 045004 (2007).
[44] The oscillations are also present for each individual flavor, nevertheless, for convenience in the visualization we sum both flavors.
[45] M. C. Bañuls *et al.*, PoS(LATTICE 2016)316 (in preparation) (2016).
[46] A. Smilga and J. J. M. Verbaarschot, Phys. Rev. D **54**, 1087 (1996).
[47] S. Dürr, arXiv:hep-th/0009094 (2000).
[48] Y. Hosotani and R. Rodriguez, Journal of Physics A: Mathematical and General **31**, 9925 (1998).
[49] C. Gattringer, T. Kloiber, and V. Sazonov, Nuclear Physics B **897**, 732 (2015).

Appendix: Density induced phase transitions in QED$_2$ - A study with matrix product states

SPIN FORMULATION

For convenience in the simulations, we use an equivalent spin formulation for the Hamiltonian from Eq. (2) obtained via a Jordan-Wigner transformation

$$\phi_k = \sum_{l<k} (i\sigma_l^z)\sigma_k^-, \qquad \phi_k^\dagger = \sum_{l<k} (-i\sigma_l^z)\sigma_k^+,$$

where we choose to order the fermions inside each site according to their flavor such that $\phi_{n,f} = \phi_{nF+f}$. In the formula above σ_j^z and $\sigma_j^\pm$ are the usual Pauli matrices acting on spin j. The Hamiltonian in spin language is given by

$$\begin{aligned} W = &- x \sum_{p=0}^{NF-1} \left(\sigma_p^+ (i\sigma_{p+1}^z) \dots (i\sigma_{p+F-1}^z) \sigma_{p+F}^- + \text{h.c.} \right) \\ &+ \sum_{n=0}^{N-1} \sum_{f=0}^{F-1} \left(\mu_f (-1)^n + \nu_f \right) \frac{1+\sigma_{nF+f}^z}{2} \\ &+ \sum_{n=0}^{N-2} \left(\frac{F}{2} \sum_{k=0}^{n} (-1)^k + \frac{1}{2} \sum_{k=0}^{n} \sum_{f=0}^{F-1} \sigma_{kF+f}^z \right)^2 , \end{aligned} \tag{S1}$$

hence for a system with N sites and F flavors of fermions, we end up with a spin chain of length NF after the transformation.

Additionally we are interested in the sector with vanishing total charge. To impose that, we add a penalty term $P = \lambda \left(\sum_{n=0}^{N-1} Q_n \right)^2$ to the Hamiltonian from Eq. (S1), where Q_n is the staggered charge given by $Q_n = \sum_{f=0}^{F-1} \frac{1}{2} \left(\sigma_{nF+f}^z + (-1)^n \right)$ in the spin formulation. The Hamiltonian including the penalty term for vanishing total charge can be implemented efficiently as matrix product operator with a bond dimension $D' = 2F + 3$, despite the long range interactions.

For our calculations presented in the main text, we chose $\lambda = 1000$ and checked the expectation value of P, where we found that it is negligible for all our simulations.

EXTRACTING THE LOCATIONS OF PHASE TRANSITIONS

Here we briefly explain how we extract the locations of the phase transitions for the two-flavor case. A short calculation shows that the Hamiltonian in the sector of vanishing total charge conserves N_0 and N_1 as well as $N = N_0 + N_1$. Hence it is block diagonal and the blocks can be labeled with $(N, \Delta N = N_0 - N_1)$. Inside a block the chemical potential terms are proportional to the identity and the Hamiltonian can be written as

$$W = \nu_0 N_0 + \nu_1 N_1 + W_{\text{aux}},$$

where W_{aux} sums up all remaining terms that are independent of the chemical potential. The ground state energy of this Hamiltonian is given by

$$E_{(N,\Delta N)}(\nu_0, \nu_1) = \nu_0 N_0 + \nu_1 N_1 + E_{\min}(W_{\text{aux}}|_{(N,\Delta N)}) \tag{S2}$$

$$= \frac{N}{2}(\nu_0 + \nu_1) - \underbrace{\frac{\Delta N}{2}}_{p_{(N,\Delta N)}} (\nu_1 - \nu_0) + E_{\min}(W_{\text{aux}}|_{(N,\Delta N)}). \tag{S3}$$

where $E_{\min}(W_{\text{aux}}|_{(N,\Delta N)})$ is a block dependent, i.e. isospin number dependent constant. From the equation above, one can immediately see that having a single value for $E_{(N,\Delta N)}(\nu_0, \nu_1)$ available inside each block is enough to determine

this constant. Moreover, Eq. (S3) reveals that for fixed N the energy inside each block only depends linearly on $\nu_1 - \nu_0$ up to a (chemical potential dependent) constant, with a slope proportional to ΔN (see Fig. S1).

A phase transition, and hence a discontinuity in the isospin number, occurs, if it is energetically favorable to go from one block characterized by $(N, \Delta N)$ to a neighboring block characterized by $(N, \Delta\bar{N} = \Delta N \pm 2)$. As discussed above, inside each block the energy scales linearly (up to a constant) with a block dependent slope. Thus a phase transition corresponds to the intersection point of the two linear functions describing the energy inside these blocks, as can be seen in Fig. S1.

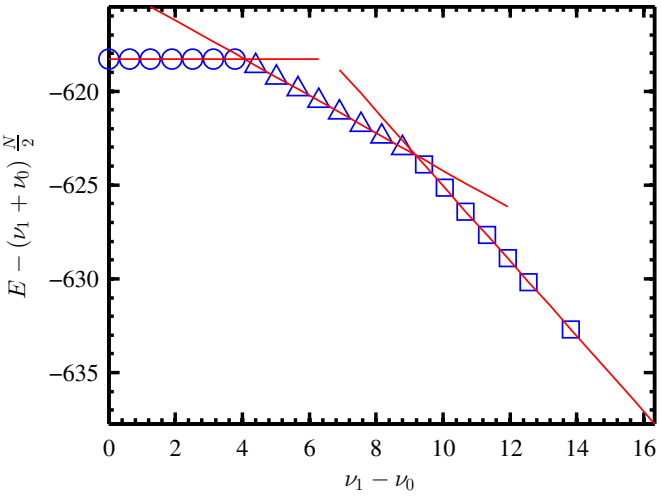

FIG. S1. (Color online) Ground state energy as a function of the chemical potential difference for $m/g = 0$, $Lg = 8$, $x = 16$, and $D = 160$. The different symbols correspond to $\Delta N = 0$ (circles), $\Delta N = 2$ (triangles) and $\Delta N = 4$ (squares). The lines represent linear functions with slope $p_{(N,\Delta N)}$.

Equating $E_{(N,\Delta N)}(\nu_0, \nu_1) = E_{(N,\Delta\bar{N})}(\nu_0, \nu_1)$ and using Eq. (S3) we can obtain the following analytical expression for the intersection points:

$$(\nu_1 - \nu_0)|_{\text{jump}} = \frac{E_{\min}(W_{\text{aux}}|_{(N,\Delta\bar{N})}) - E_{\min}(W_{\text{aux}}|_{(N,\Delta N)})}{p_{(N,\Delta\bar{N})} - p_{(N,\Delta N)}} \tag{S4}$$

$$= \frac{E_{(N,\Delta\bar{N})}(\bar{\nu}_0^*, \bar{\nu}_1^*) - \bar{\nu}_0^* N_0 - \bar{\nu}_1^* N_1 - E_{(N,\Delta N)}(\nu_0^*, \nu_1^*) + \nu_0^* N_0 + \nu_1^* N_1}{\bar{N}_0 - N_0}. \tag{S5}$$

In the second line we have explicitly substituted p and used the observation that Eq. (S2) allows to determine $E_{\min}(W_{\text{aux}}|_{(N,\Delta N)})$ ($E_{\min}(W_{\text{aux}}|_{(N,\Delta\bar{N})})$) at arbitrary values ν_0^*, ν_1^* ($\bar{\nu}_0^*$, $\bar{\nu}_1^*$). The isospin number as well as the ground state energies can be extracted from our simulations, where the former can be determined exactly as the Hamiltonian conserves N_0 and N_1. Hence the precision of $(\nu_1 - \nu_0)|_{\text{jump}}$ only depends on the precision obtained for the ground state energies. Assuming a systematic error of ΔE in the energies, one obtains for the error of the location of the phase transition

$$\Delta(\nu_1 - \nu_0)|_{\text{jump}} = \left| \frac{\partial(\nu_1 - \nu_0)|_{\text{jump}}}{\partial E_{(N,\Delta\bar{N})}(\bar{\nu}_0^*, \bar{\nu}_1^*)} \Delta E_{(N,\Delta\bar{N})}(\bar{\nu}_0^*, \bar{\nu}_1^*) \right| + \left| \frac{\partial(\nu_1 - \nu_0)|_{\text{jump}}}{\partial E_{(N,\Delta N)}(\nu_0^*, \nu_1^*)} \Delta E_{(N,\Delta N)}(\nu_0^*, \nu_1^*) \right|$$

$$= \frac{1}{\left| p_{(N,\Delta\bar{N})} - p_{(N,\Delta N)} \right|} \Big(\left| \Delta E_{(N,\Delta\bar{N})}(\bar{\nu}_0^*, \bar{\nu}_1^*) \right| + \left| \Delta E_{(N,\Delta N)}(\nu_0^*, \nu_1^*) \right| \Big). \tag{S6}$$

In practice, we select for each combination of volume and lattice spacing (Lg, x) a single data point inside of each of the phases, where we determine N_0 and N_1 and estimate the exact energy value as described in the next paragraph. Subsequently, we can compute the location of the phase transition and estimate the error using Eqs. (S5) and (S6).

EXTRAPOLATION PROCEDURE

As explained in the previous paragraph, the precision obtained for the phase transition locations crucially depends on the precision of the ground state energies. To get precise estimates for the exact energy, we extrapolate the bond

dimension $D \to \infty$. To do so, we repeat the calculation for each data point for a given combination of volume Lg, lattice spacing x and chemical potential difference $\mu_I/2\pi$ for several bond dimensions until the energy approximately scales linearly in $1/D$. For the data presented in the main text, we find that for $x \in [9, 36]$ a maximum bond dimension of $D = 160$ is enough to enter the linear scaling region, whereas for larger values of x we have to increase the bond dimension up to 220. Once we enter this regime, we take the last three data points to extrapolate linearly (see Fig. S2 for an example). As an estimate for the exact energy we take the mean value of our data point computed with the largest bond dimension, $E_{D_{\max}}$, and $E_{D=\infty}$ obtained by our extrapolation. The error is estimated as $\Delta E = \frac{1}{2}(E_{D_{\max}} - E_{D=\infty})$.

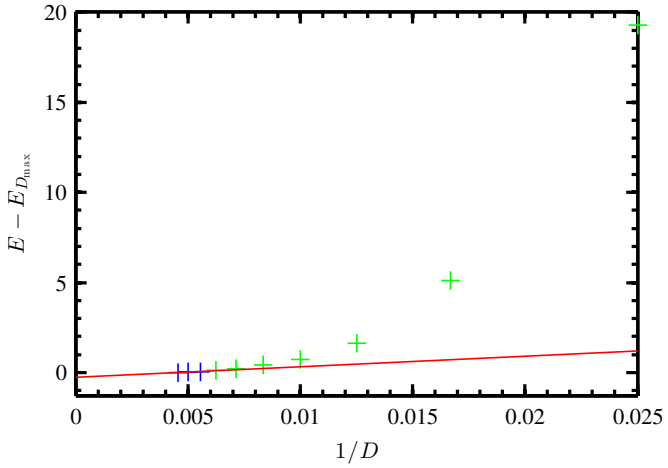

FIG. S2. (Color online) Extrapolation in bond dimension for $m/g = 0$, $\mu_I/2\pi = 0.8$, $x = 121$ and $Lg = 8$. The blue data points are the ones used for the extrapolation to the limit $D \to \infty$ and the red line shows the linear fit through the blue data points.

In a final step we can now extrapolate the estimated locations for the phase transitions, obtained by the procedure explained in the previous paragraph, to the continuum. We proceed in a standard manner and fit a second order polynomial in $1/\sqrt{x}$ and take the intersection point with the y-axis as estimate for the continuum value (see Fig. S3 for an example). As an error estimate for the continuum value, we take the fitting error where we use a 1σ confidence interval.

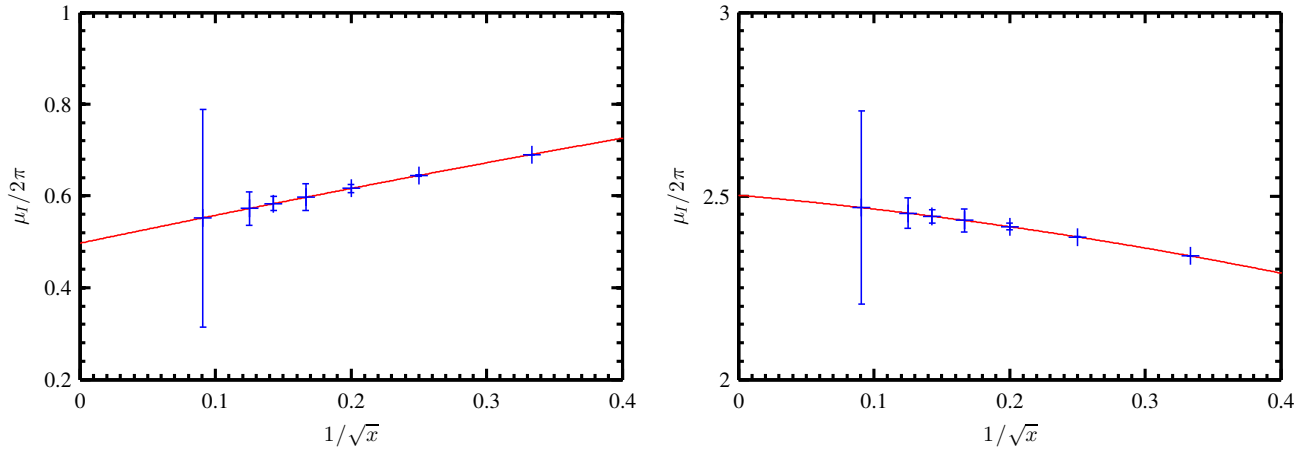

(a)Continuum limit for the location of the first phase transition. (b)Continuum limit for the location of the third phase transition.

FIG. S3. (Color online) Extrapolation of the phase transition points to the continuum for $Lg = 8$ in the massless case. The red line represents a second order polynomial fit in $1/\sqrt{x}$ and the continuum limit is estimated by taking the value of the fit function at $1/\sqrt{x} = 0$.

The final results for the location of the phase transitions obtained after the full extrapolation procedure are shown in Tab. I - IV.

Volume	1. transition	2. transition	3. transition	4. transition
$Lg = 2$	0.499960(88)	1.513345(47)	2.617208(11)	3.716041(12)
$Lg = 6$	0.499(21)	1.501(23)	2.504(22)	3.511(20)
$Lg = 8$	0.497(49)	1.501(60)	2.502(55)	3.505(51)

TABLE I. Continuum estimates for the locations of the first four phase transitions for the massless case $m/g = 0$.

Volume	1. transition	2. transition	3. transition	4. transition
$Lg = 2$	0.522620(86)	1.515910(40)	2.620237(14)	3.716558(20)
$Lg = 6$	0.711(19)	1.538(26)	2.519(23)	3.520(20)
$Lg = 8$	0.831(42)	1.575(65)	2.532(57)	3.523(52)

TABLE II. Continuum estimates for the locations of the first four phase transitions for $m/g = 0.125$.

Volume	1. transition	2. transition	3. transition	4. transition
$Lg = 2$	0.554897(76)	1.522594(40)	2.624794(14)	3.720370(19)
$Lg = 6$	0.938(16)	1.617(26)	2.558(23)	3.546(20)
$Lg = 8$	1.165(39)	1.728(66)	2.606(57)	3.571(52)

TABLE III. Continuum estimates for the locations of the first four phase transitions for $m/g = 0.25$.

Volume	1. transition	2. transition	3. transition	4. transition
$Lg = 2$	0.643234(66)	1.548542(35)	2.644094(11)	3.732926(20)
$Lg = 6$	1.402(12)	1.874(23)	2.703(22)	3.647(20)
$Lg = 8$	1.816(24)	2.168(53)	2.871(55)	3.752(49)

TABLE IV. Continuum estimates for the locations of the first four phase transitions for $m/g = 0.5$.

EFFECT OF NON-VANISHING MASS ON THE PHASE STRUCTURE

Figures 2 and 3 in the main text, as well as the Tabs. II - IV, show that for non-vanishing fermion mass the locations of the phase transitions between phases characterized by small ΔN are affected the most compared to the massless case. Transitions between phases with larger isospin number are less influenced and only slightly shifted towards higher values of $\mu_I/2\pi$. This behavior can be explained qualitatively with a change in $E_{\min}(W_{\text{aux}}|_{(N,\Delta N)})$ which is the only mass dependent contribution to the energy, as can be seen from Eqs. (S2) and (S3). Consequently introducing a non-zero value for m/g leads to a shift $\Delta E_{\min}$ with respect to the massless case, $E_{\min}(W_{\text{aux}}|_{(N,\Delta N)}) = E_{\min}(W_{\text{aux}}|_{(N,\Delta N)})|_{m/g=0} + \Delta E_{\min}$. Equation (S4) reveals that these energy shifts affect the locations of the phase transitions, as soon as they are not equal in every phase. Extracting $\Delta E_{\min}/N$ inside each phase for our smallest lattice spacing for several masses, we obtain the results shown in Fig. S4, which clearly show that the shifts are different for each phase. In particular, we see that for the phase characterized by $\Delta N = 0$, the energy shift is a lot more pronounced than for the phase characterized by $\Delta N = 2$, thus explaining the significant shift towards higher values of $\mu_I/2\pi$ for the location of the first phase transition with respect to the massless case. For phases with larger isospin number, the energy shifts differ less, consistent with the observation that the locations of the phase transitions between these phases are less affected. Although for all three volumes studied we observe similar energy shifts, Fig. 2 as well as Tabs. II - IV show that for $Lg = 2$ the locations of the phase transitions are less affected by a non-zero fermion mass. This is likely due to the finite volume effects arising from the fact that the total fermion number corresponds to the number of sites as described in the main text.

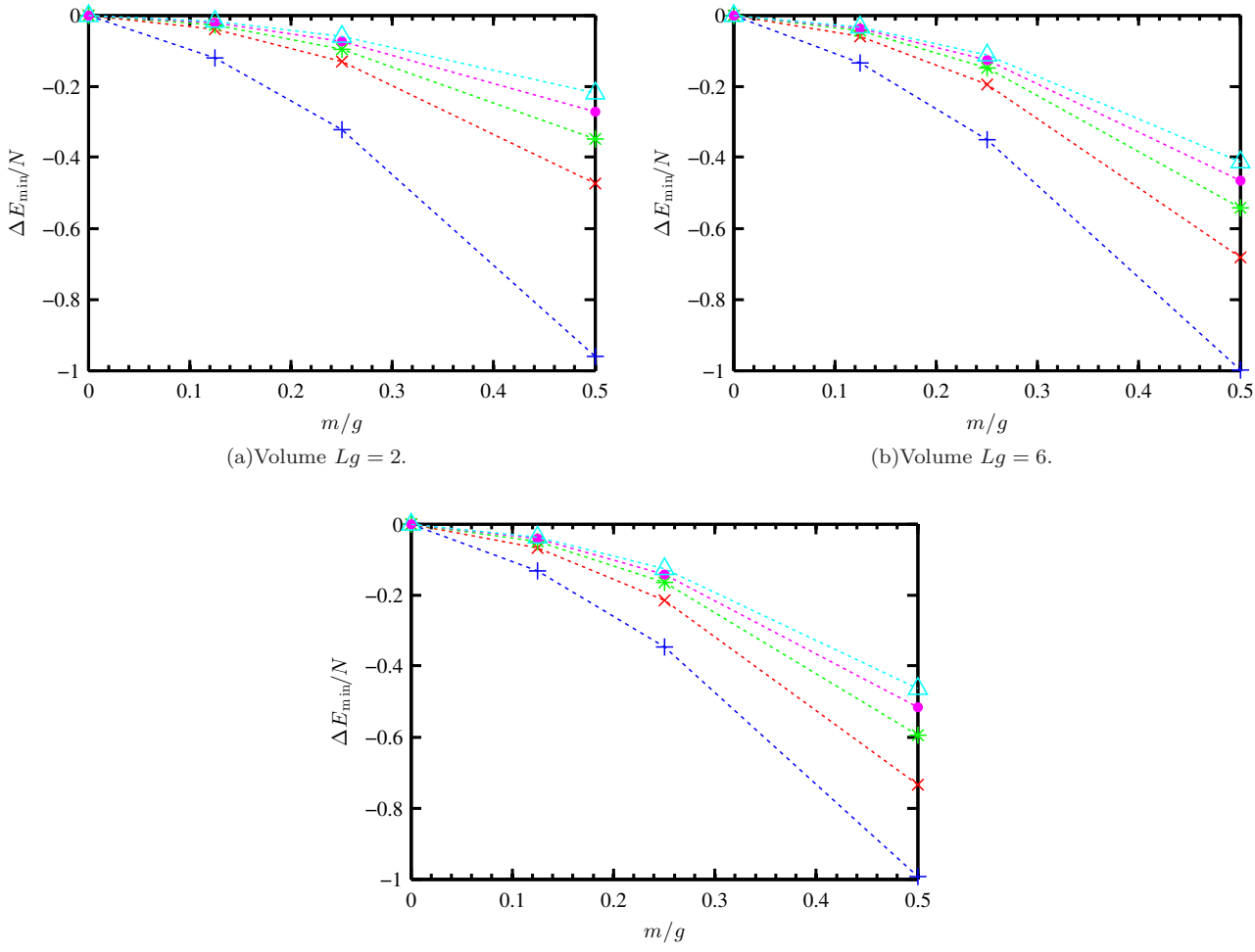

(a)Volume $Lg = 2$.

(b)Volume $Lg = 6$.

(c)Volume $Lg = 8$.

FIG. S4. (Color online) Energy shift per site $\Delta E_{\min}/N$ as a function of m/g for $x = 121$ and volumes $Lg = 2$ (a), $Lg = 6$ (b) and $Lg = 8$ (c). The different markers indicate the different phases characterized by the isospin number, blue crosses represent $\Delta N = 0$, red ✕'s $\Delta N = 2$, green asterisks $\Delta N = 4$, magenta dots $\Delta N = 6$ and cyan triangles $\Delta N = 8$. As a guide for the eye the data points are connected with dotted lines.